International Journal of Mass Spectrometry 289 (2010) 30–38

Contents lists available at ScienceDirect

International Journal of Mass Spectrometry

journal homepage: www.elsevier.com/locate/ijms

Collision induced dissociation in a flowing afterglow-tandem mass spectrometer for the selective detection of C_5 unsaturated alcohols and isoprene

Juliette Rimetz-Planchon[a,*], Niels Schoon[a], Crist Amelynck[a], Frederik Dhooghe[a,b]

[a] Belgian Institute for Space Aeronomy, Ringlaan 3, B-1180 Brussels, Belgium
[b] Department of Analytical Chemistry, Ghent University, Krijgslaan 281, S12, B-9000 Ghent, Belgium

ARTICLE INFO

Article history:
Received 13 July 2009
Received in revised form
17 September 2009
Accepted 21 September 2009
Available online 26 September 2009

Keywords:
Tandem mass spectrometry
Unsaturated alcohol
Isoprene
Collision induced dissociation
Chemical ionization

ABSTRACT

A flowing afterglow-tandem mass spectrometer (FA-TMS) was used to study a series of C_5 unsaturated alcohols and isoprene. The analytical procedure was validated through collision induced dissociation (CID) experiments on proton hydrates. In the FA, reagent H_3O^+ ions were used to chemically ionize the alcohols under study and isoprene. Chemical ionization (CI) by H_3O^+ is widely used, especially in PTR-MS instruments, and produces a main peak at m/z 69 for all studied compounds, implying the impossibility to distinguish them by a simple quadrupole mass filter. The CID of these ions at m/z 69 resulted in daughter ions with the same masses but with different intensities depending on the organic compound, the collision energy and the Ar target gas pressure in the collision cell. From these observations, pentenols were easily distinguished from methylbutenols and 3-methyl-3-buten-1-ol from the other compounds. CID experiments were also performed on the protonated alcohol, which is only a stable ion for 1-penten-3-ol, 2-methyl-3-buten-2-ol and 3-methyl-3-buten-1-ol, showing different CID patterns as a function of the collision energy. The coupling between a FA reactor and a TMS has proven to be a valuable approach to identify C_5 unsaturated alcohols and isoprene.

© 2009 Elsevier B.V. All rights reserved.

1. Introduction

Isoprene ($M = 68\ g\ mol^{-1}$), a biogenic volatile organic compound (BVOC), is emitted by a large variety of plants and constitutes 43% of all BVOCs emissions [1]. Due to extensive studies [2], it is now well known for its high reactivity and resulting impact on ozone chemistry and secondary organic aerosol (SOA) formation [3,4]. Among C_5 unsaturated alcohols ($M = 86\ g\ mol^{-1}$), 2-methyl-3-buten-2-ol (232MBO) was found to be directly emitted by some pine species [5–8]. Even though the geographic area of 232MBO biogenic emitters is restricted (for example, based on 1992–1993 data, needle forests are estimated to represent only 4.1% of the global land cover [9]), 232MBO can have implications on regional atmospheric chemistry [10], since it is highly reactive with the main atmospheric oxidants [11,12]. Next to being emitted by vegetation, 232MBO is also a pheromone produced by the spruce bark beetle [2]. Formation of SOA from degradation products of 232MBO is a more controversial issue [13]. Isomers of 232MBO were also investigated. König et al. [14] detected low emission rates of 1-penten-3-ol (1P3OL) and 2-penten-1-ol (2P1OL) by rye and of 1P3OL, 2P1OL, 3-methyl-3-buten-1-ol (331MBO) and 3-methyl-2-buten-1-ol (321MBO) by rape. In addition, plants exposed to physical damage can produce 1P3OL and 2P1OL [14–16].

Isoprene can be detected by photoionization (at 10.7 eV) but this technique suffers from interferences from other hydrocarbons [2,17]. The Fast Isoprene Sensor, based on chemiluminescence, has also been employed to specifically quantify isoprene in real-time without preconcentration step prior to analysis [18,19]. At present, however, two main techniques are widely used for the detection and/or the quantification of isoprene and C_5 unsaturated alcohols: (i) gas chromatography combined with various detection methods (GC-FID, GC–MS) [6,8,20–23], which allows a sensitive and selective analysis of BVOCs in complex mixtures, but suffers from poor time resolution. (ii) Chemical ionization mass spectrometry (CIMS), which is a fast and sensitive technique to monitor BVOCs on-line, but which often lacks selectivity.

Nowadays proton transfer reaction-MS (PTR-MS) is certainly the most frequently used CIMS instrument [15,24–26]. Other CIMS instruments are also used to investigate C_5 unsaturated alcohols, like proton transfer reaction-ion trap mass spectrometry [27], chemical ionization reaction-time-of-flight mass spectrometry [28] and flowing afterglow-selected ion flow tube-mass spectrometry (FA-SIFT-MS) in positive [29,30] and negative ion modes [31,32].

The main disadvantage of CIMS techniques is the possibility of overlapping CI product ion masses originating from different compounds and several methods were developed to overcome the

* Corresponding author. Tel.: +32 2 373 03 77; fax: +32 2 373 84 23.
E-mail address: Juliette.Rimetz@aeronomie.be (J. Rimetz-Planchon).

1387-3806/$ – see front matter © 2009 Elsevier B.V. All rights reserved.
doi:10.1016/j.ijms.2009.09.008

resulting lack of selectivity. GC has for instance been used in parallel and in series with PTR-MS [15,26,33]. Williams et al. [26] used a water trap to remove methanol and C_5 alcohols and therefore to discriminate isoprene from C_5 unsaturated alcohols. The authors also took into account correlations between isoprene and its oxidation products to exclude the presence of C_5 unsaturated alcohols in samples. Karl et al. [25] quantified the individual contribution of isoprene and 232MBO by the ratio of ion signals at m/z 69 and m/z 87. CI is generally performed with H_3O^+ but the use of other CI reagents can be a possible way to differentiate isobaric species [29–32]. Finally, the collision induced dissociation (CID) patterns of CI product ions can be different for isobaric and isomeric organic compounds [34].

In atmospheric chemistry, CID is generally performed in an ion trap included in different configurations such as a PIT-MS [35–38], a PTR-linear ion trap [39] or a membrane inlet mass spectrometer [40], and more rarely in the collision cell of a tandem MS instrument (TMS) [41–43]. FA-TMS is often employed in fundamental chemistry to characterize ion structures and to obtain thermodynamic information [44–47]. The present study explores the capabilities of a newly built FA-TMS instrument for selective detection of isomeric compounds, more particularly of six isomeric C_5 unsaturated alcohols and isoprene. The discrimination is expected to be possible based on the combination of CI by H_3O^+ and compound-specific CID patterns occurring in the collision cell.

2. Materials and method

2.1. FA-TMS

The FA-TMS instrument consists of a home-made flowing afterglow reactor, which is coupled to a TMS custom-designed by Extrel CMS (Pittsburgh, USA), and is shown in Fig. 1.

The stainless steel flow tube reactor has a radius of 2 cm and a length of about 1 m. Argon is pumped through the reactor with a flow rate of 2.5×10^{-5} STP m^3 s^{-1} (at standard conditions of pressure (1013.25 hPa) and temperature (273.15 K)) by means of a Roots pump, resulting in a reactor pressure of 0.6 hPa. Formation of reactant ions is initiated by ionization of Ar atoms by impact of electrons emitted by an emission current-regulated thoriated iridium filament.

H_3O^+ reactant ions are produced through a sequence of ion/molecule reactions, starting with the reactions of Ar^+ and Ar_2^+ ions with water vapour, which is introduced in controlled amounts at 17 cm downstream the filament. The water flow is optimized to obtain the highest intensity of H_3O^+, a full conversion of Ar^+ and Ar_2^+ to H_3O^+ at the location where the reactant BVOC is introduced, and a minimal contribution of higher order proton hydrates ($[H_3O^+{\cdot}H_2O]/[H_3O^+] \approx 11\%$ at the downstream end of the flow tube). Small leaks in the flow tube and/or the presence of trace amounts of oxygen in the buffer gas result in a small contribution of $O_2^{\bullet+}$ impurity ions ($[O_2^{\bullet+}]/[H_3O^+] \approx 4\%$).

In order to decrease ion loss in the flow tube through electron/positive ion recombination, 2.3×10^{-8} STP m^3 s^{-1} of a 1000 ppm SF_6/Ar mixture is added through an inlet situated at about 9 cm downstream the filament to scavenge thermal electrons [48]. Finally, small flows of dilute mixtures of BVOCs in He (about 1/1000 BVOC/He), stored in a 5×10^{-3} m^3 glass reservoir, are introduced in the FT at 38 cm upstream of the mass spectrometer inlet and CI product ions are formed by reaction of these BVOCs with the reactant ions. Reactant and CI product ions are at their ground state through collisions with the buffer gas.

Reactant and CI product ions are then sampled into a first vacuum chamber through an orifice (1 mm diameter) in an electrically insulated interface flange between the medium-pressure reactor and the vacuum chamber. This cube-shaped vacuum chamber is pumped by a 1.6 m^3 s^{-1} turbomolecular pump and the pressure obtained in operating conditions is 1.4×10^{-4} hPa. An extraction potential (−5 V dc) is applied to the interface flange to improve the ion signal intensity and stability [45]. By means of an Einzel lens system, ions entering the vacuum system are guided towards a quadrupole deflector, which is located in a second, T-shaped, vacuum chamber which is pumped differentially by a 0.5 m^3 s^{-1} turbomolecular pump, resulting in a pressure of 2×10^{-7} hPa. The quadrupole deflector bends the ion beam by 90° resulting in a clean separation of ions from photons, metastables, particulate and non-ionized molecular beam gases, and thus provides a better signal-to-noise ratio.

The ions are subsequently introduced in the TMS probe which is located in the main vacuum chamber. The TMS is used in two modes. In Q1MS mode, the first quadrupole Q1 operates in full scan whereas Q2 acts as an ion guide. This mode allows for example the observation of all ions generated in the FA and entering the TMS. In MS/MS mode, the ions entering Q1 are selected according to their m/z ratio. The preselected ions (called parent ions) are subsequently injected in O, which is filled with a collision gas (Ar) at low pressure (a few 10^{-4} hPa). At sufficiently high collision energies of the reactant partners, CID of the parent ions entering the collision cell results in one or more daughter ions. The fragmentation spectrum is finally obtained by scanning Q2 over the useful mass range and the ions are detected with a secondary electron multiplier.

The rods have a diameter of 19 mm for Q1 and Q2 and of 3 mm for O, and a length of 210.8 mm for Q1 and Q2 and 200 mm for O. The diameter of the entrance and exit orifice of O is 13 mm. The multipole assemblies are driven by independent power supplies with frequencies of 880 kHz, 2.1 MHz and 880 kHz for Q1, O and Q2 respectively. O operates in radio-frequency (RF)-only mode, so as an ion guide. The nominal mass ranges are 1–1000 amu, 1–500 amu, and 1–1000 amu for Q1, O and Q2 respectively. The main vacuum chamber, containing Q1, O, Q2 and the detector is pumped by a set of turbomolecular pumps with a total pumping speed of 2 m^3 s^{-1}. The pressure in this chamber varies from 4×10^{-8} hPa (no target gas) to 9×10^{-6} hPa, which corresponds to the maximum pressure condition used in the collision cell, i.e., 6.7×10^{-4} hPa.

The housing of Q1 is set at a fixed value of −2 V, whereas the housing of O and Q2 are at the same potential which can be varied during experiments. Q1 and Q2 are provided with pre- and post-filters to reduce fringing fields and optimize ion transmission. A Q1 entrance lens (15.2 mm diameter aperture) focuses ions on the axis of Q1 and reduces rf fringing field effects. Interquad lenses (12.7 mm diameter aperture) located between Q1 and O and between O and Q2 guide the ion beam in the gap between the multipoles. Finally, a Q2 exit lens (15.2 mm diameter aperture) focuses the ions towards the detector. The entire TMS instrument is controlled by means of commercial software (Merlin) provided by the TMS manufacturer (Extrel).

2.2. Methodology and its validation based on proton hydrates experiments

During real-time data acquisition, a window that includes the total peak area is determined for each peak. Considering peak area instead of peak height allows to take into account asymmetric peaks, as is the case for parent ions at high collision energy. Averages over at least 7 scans were considered. Corrections applied to the raw data take into account the temporal shift of signal intensities, the background and the mass discrimination linked to the use of different multiplier voltages of the detector. Mass discrimination occurring in Q2 cannot be evaluated but does not affect the final conclusions, since all experiments were performed at the same conditions. The temporal shift is caused by the shift in reac-

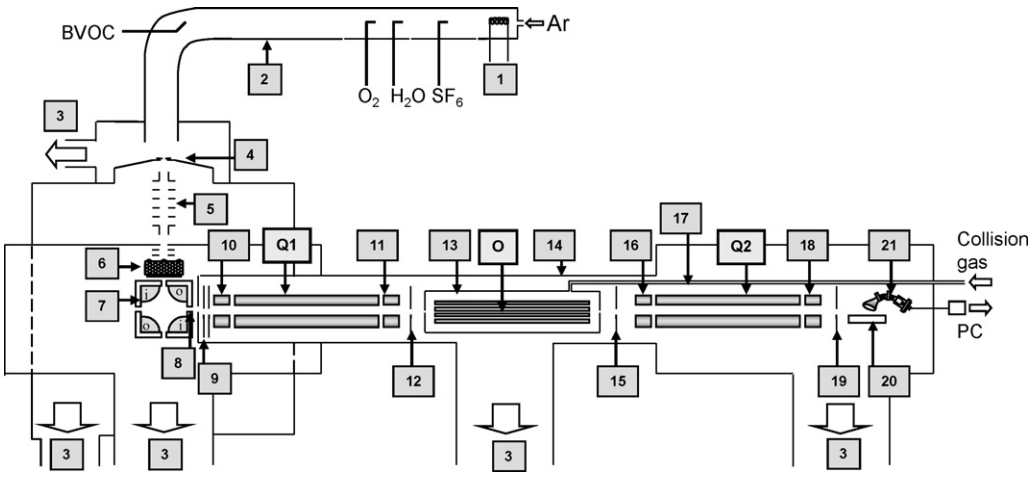

Fig. 1. Schematic representation of the FA-TMS instrument. [1] Electron emitting filament, [2] flow tube (FT), [3] to pumping system, [4] interface plate, [5] lens system, [6] internal ion source (not used), [7] ion deflector (i, inner poles; o, outer poles), [8] deflector exit lens, [9] Q1 entrance lens, [10] Q1 pre-filter, [Q1] first quadrupole, [11] Q1 post-filter, [12] Q1/O interquad lens, [13] collision cell, [O] octopole, [14] main vacuum chamber, [15] O/Q2 interquad lens, [16] Q2 pre-filter, [Q2] second quadrupole, [17] collision gas inlet, [18] Q2 post-filter, [19] exit lens, [20] discrete dynode, [21] electron multiplier.

tant gas flow due to the decrease of the total pressure of the BVOC mixture in the glass bottle in the course of the experiments, and by the long-term fluctuations of the reactant ion production in the flow tube. Background was recorded for each experiment and was calculated as the average of the baseline. These background values are independent of m/z over the m/z range studied and have been subtracted from the raw data. Analytical detection limit was calculated as three times the standard deviation on the baseline and only data above the analytical detection limit were considered. Background values and analytical detection limits depend on the width of the peak and on the collision energy. Worst values are met for the largest peak at the highest collision energy. The nature of the reactant gas does not seem to have any influence.

Experiments were carried out at different collision energies in the center-of-mass frame of reference (E_{CM}), calculated by Eq. (1). The laboratory collision energy (E_{LAB}) is the difference between the stopping potential (V_{STOP}) and the dc level (also called pole bias or rod offset) of the octopole (O_{PB}) [49]. V_{STOP} is defined as the potential that the ions experience at the location of their last collision with the Ar buffer gas atoms of the FA, which is very close to the orifice of the interface flange. V_{STOP} was determined by retarding the parent ions entering O by changing O_{PB} and measuring the corresponding strength of the remaining parent ion signal. The retarding curve was fitted and differentiated, giving a bell-shaped curve with a maximum corresponding to V_{STOP}, and a full width at half maximum (FWHM) showing the energy spread of the ions entering O [50,51]. Identical results for the stopping potential were obtained by retarding the ions in Q2, i.e., by changing $Q2_{PB}$.

$$E_{CM} = E_{LAB} \times \frac{M_{Ar}}{M_{Ar} + M_{parent}} \quad (1)$$

The voltages of the electrostatic lenses upstream O and on the Q1 housing, as well as the rod offsets of Q1 pre-, post-, and main filters were optimized to obtain an intense and symmetric parent signal. $Q1_{PB}$ was fixed at −4.5 V. The same optimization was used for all ions studied. O_{PB} controls the collision energy and was varied between −4 V and −35 V during the experiments. No experiments were performed at lower collision energies, since parent ion peaks then become too wide due to an excess velocity in the transition region between Q1 and O [52]. Special care was taken to optimize $Q2_{PB}$ and the potentials of all lenses and filters downstream the octopole. These potentials were chosen to be slightly more negative than O_{PB} to ensure that both unreacted parent ions and fragments reach the detector [51] and have symmetric peak shapes.

To validate the instrumental parameter settings, the break-up patterns of proton hydrates were studied. The collision induces simple dissociation through the loss of one or more water molecules. Experiments were performed at 1.5×10^{-4} hPa and 6.7×10^{-4} hPa of Ar in the collision cell. The curves in Fig. 2 present the fragment ions intensities, relative to the initial intensity of the parent ion introduced in the collision cell, as a function of E_{CM}. Fragment ions are easily observed and appear at E_{CM} values close to the

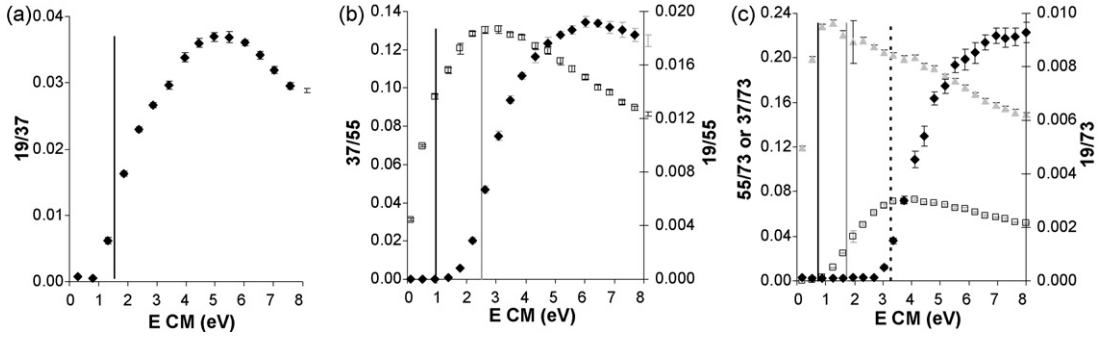

Fig. 2. Evolution, as a function of E_{CM}, of fragment ions intensity at m/z 19 (♦), m/z 37 (□) and m/z 55 (▲), relative to the initial parent ion intensity [a] $H_3O^+{\cdot}H_2O$ (m/z 37), [b] $H_3O^+(H_2O)_2$ (m/z 55) and [c] $H_3O^+(H_2O)_3$ (m/z 73). Vertical lines represent the minimum of energy required to detach one (black), two (grey) or three (dotted) water molecules [49]. Collision cell pressure = 1.5×10^{-4} hPa.

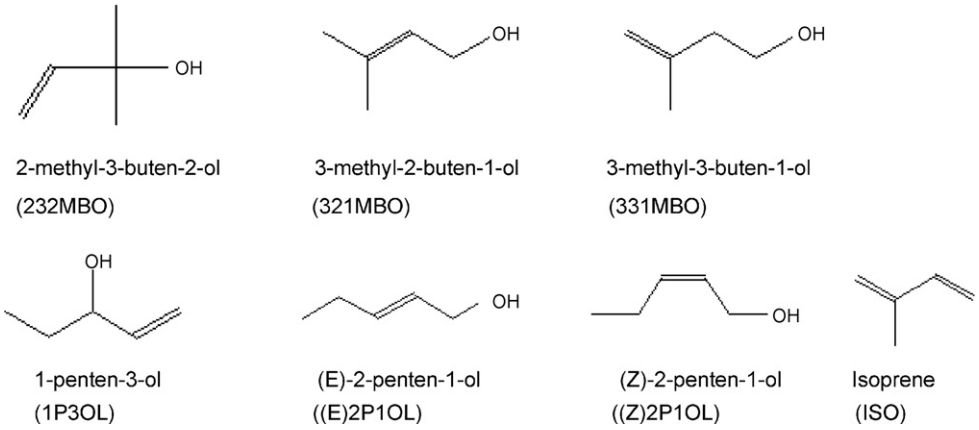

Fig. 3. Schematic representation of the BVOCs studied and their abbreviation used in the text.

minimal energy required to detach water molecules from vibrationally cold clusters [49]. The energy required to detach one water molecule from $H_3O^+(H_2O)_n$ ($n = 2$ and 3) is very low, which explains the difference between the experimental and the theoretical values. Dawson [49] explained this difference by the difficulty to correctly measure low E_{CM} values. In agreement with the observations by Dawson [49], ion signals at m/z 37 and m/z 19 in Fig. 2c display a linear rise for E_{CM} above the threshold energy to reach a saturated yield at about 4 eV and 8 eV for m/z 37 and m/z 19 respectively. The saturated yield of ion signals at m/z 55 was obtained at roughly 1 eV, in agreement with Dawson [49].

2.3. Chemicals used

Six unsaturated monohydroxylic isomeric C_5 alcohols and isoprene were studied (Fig. 3). (*E*)-2-penten-1-ol (95%) ((*E*)2P1OL), 3-methyl-3-buten-1-ol (97%) (331MBO), 2-methyl-3-buten-2-ol (98%) (232MBO) and isoprene (>99.5%) (ISO) were obtained from the Sigma–Aldrich Company. (*Z*)-2-penten-1-ol (98%) ((*Z*)2P1OL), 1-penten-3-ol (99%) (1P3OL) and 3-methyl-2-buten-1-ol (99%) (321MBO) were purchased from Acros Organics. The argon buffer gas (99.9997%) and the 1000 ppm SF_6/Ar mixture were obtained from Air Products.

3. Results and discussion

3.1. Ions produced in the FA

For all compounds, the major product ion from CI by H_3O^+ was observed at m/z 69 ($C_5H_9^+$), which is consistent with previous studies [26,29,30,53,54]. It results from protonation of the hydroxyl group followed by a loss of one water molecule $[M+H-H_2O]^+$

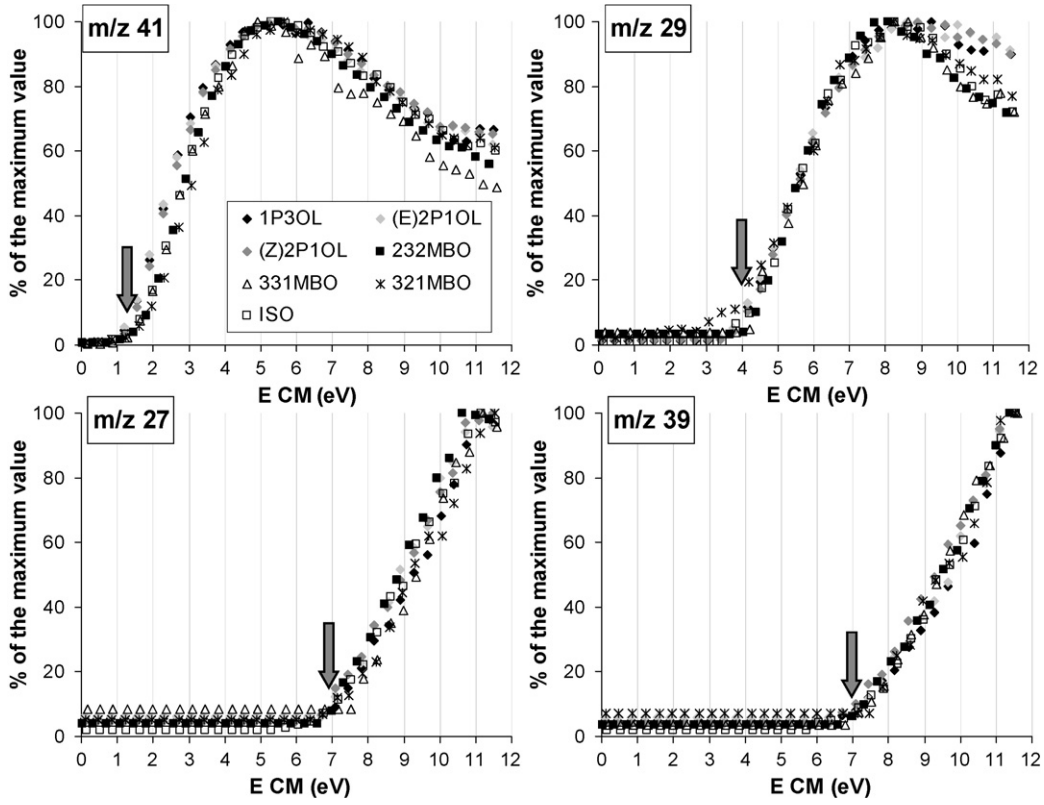

Fig. 4. Intensity of fragments m/z 41, m/z 29, m/z 27 and m/z 39 from the CID of m/z 69, relative to their maximum of intensity measured, as a function of E_{CM}, for each of the compounds studied, at 1.5×10^{-4} hPa. Arrows indicate an estimation of the appearance potentials.

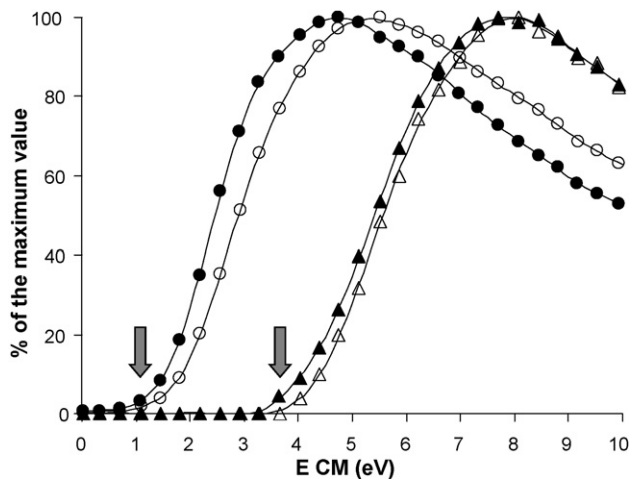

Fig. 5. Intensity of fragments at m/z 41 (circles) and at m/z 29 (triangles) from the CID of m/z 69 ions, relative to their maximum intensity measured, as a function of E_{CM}, for 232MBO at two Ar pressures in the collision cell: 1.5×10^{-4} hPa (hollow symbols) and 6.7×10^{-4} hPa (full symbols). Arrows indicate an estimation of the appearance potentials.

for C_5 alcohols [55,56] and corresponds to the protonated compound $[M+H]^+$ for isoprene [57]. The protonated alcohol at m/z 87 ($C_5H_{10}O{\cdot}H^+$) was observed for 1P3OL, 331MBO and 232MBO. Schoon et al. [30] noted that $[M+H]^+$ was not observed when the double bond was located in the "2" position, which is the case for 321MBO and 2P1OL. The protonation can occur on a sterically accessible C=C double bond, as it is the case for 1P3OL, 232MBO and 331MBO (double bond located in terminal position). Ions at m/z 87 were also observed for isoprene, and were attributed to $[M+H+H_2O]^+$ as a result of excess H_2O in the FA.

3.2. Break-up pattern of ions at m/z 69 produced by H_3O^+/molecule reactions as a function of the collision energy and the Ar pressure in the collision cell

The stopping potentials (V_{STOP}) and the FWHM of the collision energy were found to be -3.8 ± 0.2 (1σ, $n = 8$) V and 1.9 ± 0.3 (1σ, $n = 8$) V respectively. In these experiments, the range of applied E_{CM} values was 0.1–11.5 eV. The CID fragmentation patterns of m/z 69 ions from the seven BVOCs as a function of E_{CM} are presented in Fig. 4. Depending on E_{CM}, break-up produces major fragment ions at m/z 41 and m/z 29 and minor ones at m/z 27, m/z 39 and m/z 53. Ions at m/z 53 were not investigated because of both their very low intensity and their small E_{CM} window of observation: this ion appears at $E_{CM} > 4.5$ eV and, at high E_{CM} values (about 9.6 eV), there is an interference with the tail of the parent ion peak, which is oriented toward lower m/z values.

Table 1
Dataset and terms used for the calculation of $R_{X/Y}$ and its associated uncertainty u_{total}.

Replicate	i (i = 1 to n)
Intensity I at $m/z = X$	$I_{X,i}$
Standard deviation associated to I_X	$\sigma_{X,i}$
Intensity at $m/z = Y$	$I_{Y,i}$
Standard deviation associated to I_Y	$\sigma_{Y,i}$
Ratio $R_{X/Y}$ of intensities I_X/I_Y	$R_{X/Y,i}$
Uncertainty associated to $R_{X/Y}$	u_i

Appearance potentials are the minimum E_{CM} needed to observe fragments. The determination of the accurate values, however, requires theoretical models [58,44] and has not been performed in our study. At 1.5×10^{-4} hPa or 6.7×10^{-4} hPa of Ar in the collision cell, the experimental appearance potentials are the same for all compounds studied: 1.0–1.6 eV (for m/z 41), 3.5–3.8 eV (for m/z 29) and 6.3–6.8 eV (for m/z 27 and m/z 39) (Fig. 4). So, these values cannot be used to discriminate the different gases. The Ar pressure in the collision cell can have an influence on the appearance potentials, such as a shift to lower potentials with increasing collision cell pressure. This phenomenon is caused by multiple collisions providing additional energy. Small (0.2–0.3 eV for both m/z 41 and m/z 29 ions) but significant shifts of the appearance curves are observed between experiments performed at 1.5×10^{-4} hPa and 6.7×10^{-4} hPa (Fig. 5).

At the Ar collision cell pressures used in the present experiments, an E_{CM} value of about 1.0 eV is sufficiently high for m/z 69 ions to fragment to m/z 41 ions ($C_3H_5^+$) with a neutral loss of C_2H_4 (Fig. 4). The associated mechanism could be heterolytic cleavage with or without proton migration. Within experimental uncertainties, intensities of m/z 41 peaks are comparable for all seven BVOCs (Fig. 6). From about 3.5 eV, m/z 29 fragment ions appear ($C_2H_5^+$). These ions originate from direct break-up of m/z 69 ions, with a neutral loss of C_3H_4. From about 6.3 eV, peaks at m/z 27 ($C_2H_3^+$) and at m/z 39 ($C_3H_3^+$) appear in the mass spectra. The fragment ions at m/z 27 can be formed by both direct fragmentation of parent ions with a loss of C_3H_6 and sequential CID via a loss of H_2 from m/z 29 fragment ions. Fragment ions at m/z 39 can result from fragmentation of both m/z 69 and m/z 41 ions, with a loss of C_2H_6 and H_2, respectively. In the case of ISO, Maleknia et al. [59] also observed an abundant ion at m/z 39 by PTR-MS analysis, attributed to the fragmentation of the protonated isoprene with a loss of C_2H_6. Discrimination between direct and sequential CID mechanisms cannot be confirmed with our analytical tools and needs complementary techniques [60].

When considering intensities of fragments ions, three groups of compounds can be observed (Fig. 6): (1) pentenols, with the highest m/z 29 and intermediate m/z 27 peak intensities, (2) 232MBO, 321MBO and ISO, with intermediate m/z 29 and

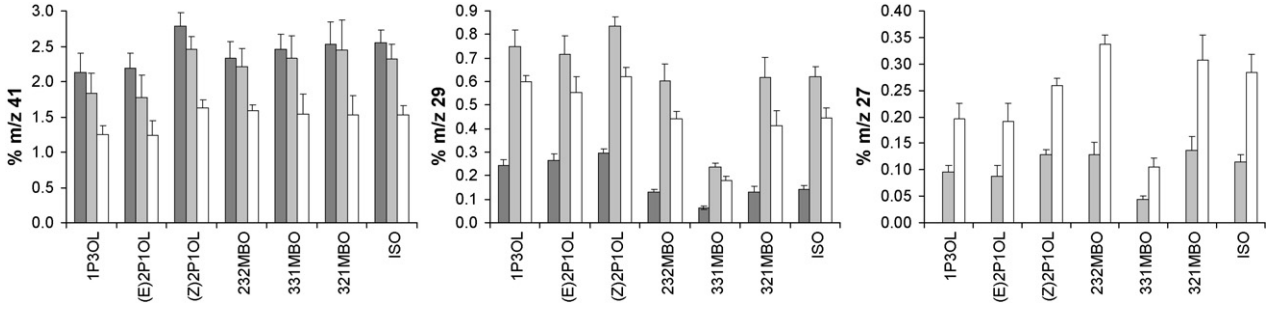

Fig. 6. Fragments intensities at m/z 41, m/z 29 and m/z 27 relative to the initial m/z 69 intensity for the compounds studied at 1.5×10^{-4} hPa and at three E_{CM} values: 4.8 eV (dark grey), 8.2 eV (light grey) and 10.7 eV (white).

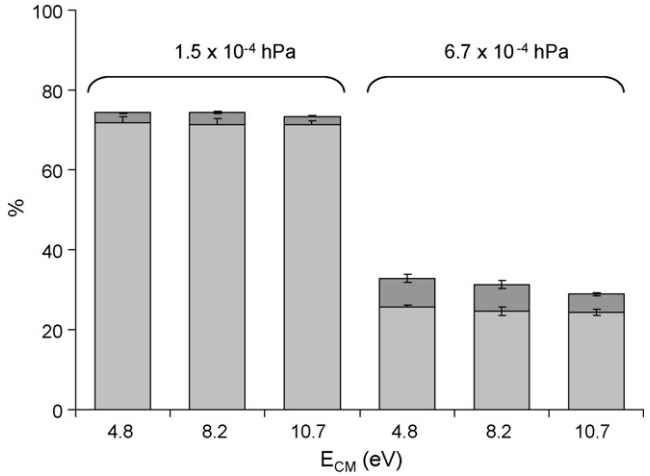

Fig. 7. Percentages of fragment ions (dark grey) and unfragmented parent m/z 69 ions (grey) relative to the initial parent ion intensity, at 1.5×10^{-4} hPa and 6.7×10^{-4} hPa collision gas pressures and at three E_{CM} values.

the highest m/z 27 peak intensities, and (3) 331MBO, with clearly the lowest m/z 29 and m/z 27 peak intensities. With the exception of stereochemical differences around the double bond, resonant forms of m/z 69 ions from pentenols are identical (CH_3—CH_2—CH=CH—$CH_2^+ \leftrightarrow CH_3$—$CH_2$—$CH^+$—CH=$CH_2$). 232MBO and 321MBO also have similar resonant forms ((CH_3)$_2$—C=CH—$CH_2^+ \leftrightarrow$ (CH_3)$_2$—C^+—CH=CH_2). In the case of 331MBO, only one form is possible (CH_2=C(CH_3)—CH_2—CH_2^+). Consequently, similar resonant forms of m/z 69 ions could explain similar fragmentation patterns for alcohols included in each group.

In addition to bond cleavages, many rearrangements can occur due to the presence of the double bonds, explaining the difference observed in fragmentation patterns between groups. Buhr [61] for instance propose a mechanism for the acyclic unsaturated alcohols 3-hexen-1-ol and 1-octen-3-ol, for which intramolecular rearrangements can occur prior to fragmentation. Because of the possible occurrence of such rearrangements, unambiguous identification of fragmentation mechanisms of the m/z 69 ion, based solely on our experimental results, remains a difficult task to perform.

3.3. Ratio between ion signals at different m/z value as a parameter to discriminate isobaric ions

A systematic study was carried out on the most abundant ion at m/z 69 from CI by H_3O^+ in order to distinguish BVOCs based on ions intensity ratios and their associated uncertainties. For the seven BVOCs studied, three E_{CM} values (4.8 eV, 8.2 eV and 10.7 eV) at two Ar collision cell pressures (1.5×10^{-4} hPa and 6.7×10^{-4} hPa) were applied, i.e., 42 conditions in total. For each condition, at least $n = 6$ replicates i were performed, with i the individual replicate. Let's consider a given condition and two ions at m/z X and m/z Y. Data treatment consisted in calculating the ratio $R_{X/Y}$ of intensities at m/z X and m/z Y and its associated total extended uncertainty u_{total} (Table 1). The ratio $R_{X/Y}$ corresponds to the arithmetic mean of $R_{X/Y,i}$ of the n experimental replicates i. To calculate u_{total}, both the uncertainty associated to $R_{X/Y}$, called u (arithmetic mean of u_i, Table 1),

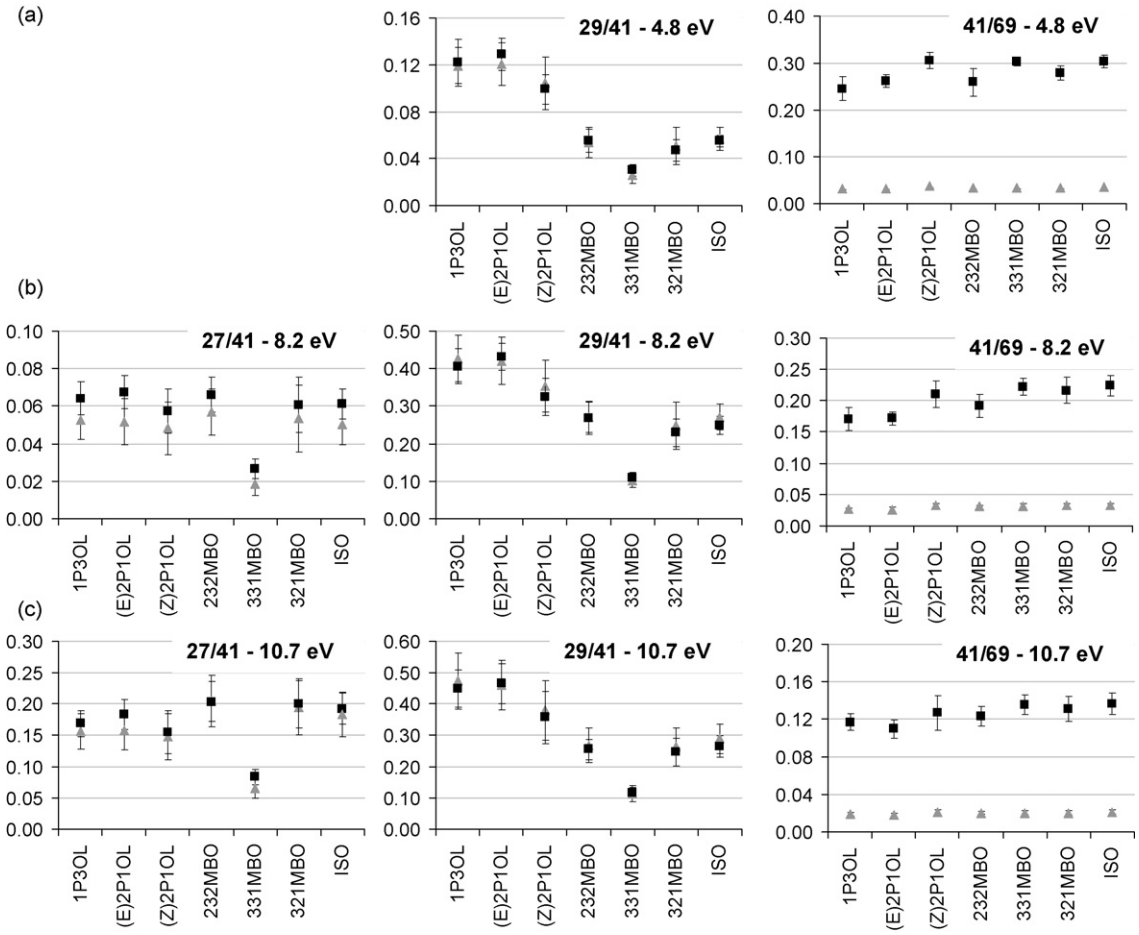

Fig. 8. Ratios 29/41, 27/41 and 41/69 for each compound at 1.5×10^{-4} hPa (grey triangles) and 6.7×10^{-4} hPa (black squares), and at three E_{CM} values: [a] 4.8 eV, [b] 8.2 eV and [c] 10.7 eV. Intensities at m/z 69 correspond to the unfragmented parent ions.

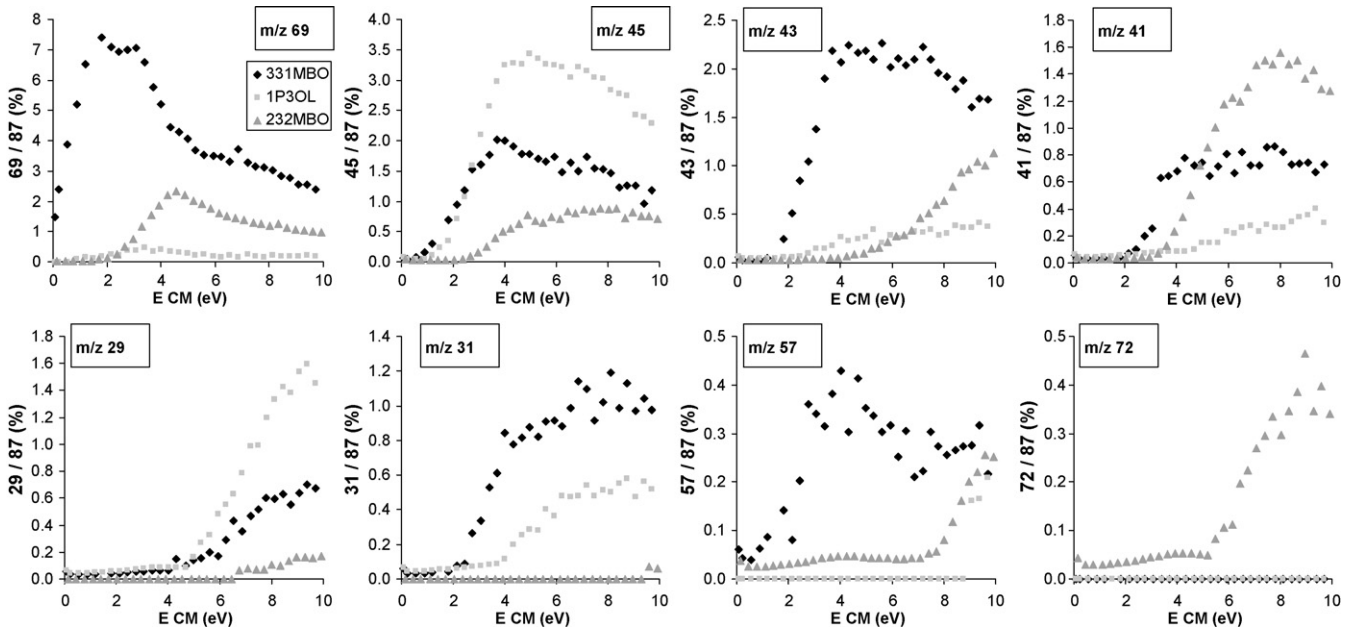

Fig. 9. Intensity of fragments relative to the intensity of initial parent ion m/z 87 (in percentage) as a function of E_{CM} for 331MBO, 1P3OL and 232MBO at 1.5×10^{-4} hPa.

and repeatability, called r, were taken into account. The terms u_i, r and u_{total} were calculated following Eq. (2)–(4) respectively. The factor 2 in Eq. (4) corresponds to the coverage factor at the 95% level of confidence.

The ratios $R_{27/41}$, $R_{29/41}$, $R_{27/69}$, $R_{29/69}$ and $R_{41/69}$ and their uncertainties were calculated. Repeatability (r) varies from 0.1 to 9%, with a mean of 3%. Lowest and highest total extended uncertainties (u_{total}) are found for $R_{41/69}$ (major peaks) and $R_{27/41}$ (m/z 27 is a minor peak) respectively.

$$u_i = \frac{I_{X,i}}{I_{Y,i}} \left(\frac{\sigma_{X,i}}{I_{X,i}} + \frac{\sigma_{Y,i}}{I_{Y,i}} \right) \quad (2)$$

$$r = \sqrt{\frac{1}{(n-1)n} \sum_{i=1}^{n} (R_{X/Y,i} - R_{X/Y})^2} \quad (3)$$

$$u_{total} = 2 \times \sqrt{u^2 + r^2} \quad (4)$$

Collection efficiencies were calculated following Eq. (5). They do not depend on the studied compound or E_{CM} but they decrease when Ar pressure in the collision cell increases, with 74 ± 2 (1σ, $n = 139$)% and 31 ± 2 (1σ, $n = 107$)% at 1.5×10^{-4} hPa and 6.7×10^{-4} hPa, respectively. The "loss" may be attributed to discrimination effects linked to mass, energy or scattering angles [62], but is not really a problem since all experiments were carried out with the same conditions.

$$\text{collection efficiency}\,(\%) = 100 \times \frac{(\text{fragments} + \text{parent})_{\text{Ar introduced in the collision cell}}}{\text{parent}_{\text{No Ar in the collision cell}}} \quad (5)$$

However, the sum of all fragment ion signals represents only 3% and 6% of the initial intensity of the ion signal at m/z 69 (i.e., when no Ar was introduced in the collision cell) at 1.5×10^{-4} hPa and 6.7×10^{-4} hPa respectively (Fig. 7). Consequently, some sensitivity problems could be imagined in the case of real atmospheric samples containing traces of BVOCs.

All ratios for all experimental conditions are presented in Fig. 8. The Ar pressure does not have a large influence on the ratios $R_{27/41}$ and $R_{29/41}$ (fragments), in agreement with observations from Steeghs et al. [35] concerning the acetone fragment ion ratio $R_{41/31}$. Ratios of fragment ion signals to the unfragmented parent ion signal at m/z 69 are lower at 1.5×10^{-4} hPa than at 6.7×10^{-4} hPa. These last ratios provide additional information but these experiments must be carried out at exactly the same pressure. The 331MBO isomer can be easily distinguished from the other compounds studied, since it has the lowest ratios, except for $R_{41/69}$. It is clearly possible to identify pentenols from MBOs and isoprene, especially from the ratios $R_{29/41}$ (at the two pressures) and $R_{29/69}$ (at 6.7×10^{-4} hPa, not shown) at E_{CM} equals to 4.8 eV. The ratio $R_{29/69}$ at 4.8 eV and at 6.7×10^{-4} hPa (not shown) may be used to identify isoprene and 232MBO, even if the difference is small. In the same way, (*Z*)2P1OL may be distinguished from the two other pentenols by the ratio $R_{41/69}$ at 6.7×10^{-4} hPa, and at 4.8 eV and 8.2 eV.

3.4. Break-up of the protonated alcohol as an alternative to discriminate isomers

CI by H_3O^+ produces ions at m/z 87 for only 1P3OL, 331MBO and 232MBO. The ion signal at m/z 87 was used in some PTR-MS studies to identify 232MBO [24,25]. CID of ions at m/z 87 provides different fragment ions, with different intensities and occurring at different collision energies. The mean collection efficiency was 67% and 37% for experiments at 1.5×10^{-4} hPa and 6.7×10^{-4} hPa, respectively. Main CID fragment ions were observed at m/z 69 ($C_5H_9^+$, due to the loss of one water molecule) and at m/z 45 ($C_2H_5O^+$, due to the neutral loss of C_3H_6). Minor fragments were detected at m/z 29,

Table 2
Range of appearance potential (in eV) of fragment ions from CID of protonated 331MBO, 1P3OL and 232MBO at 1.5×10^{-4} hPa.

m/z	331MBO	1P3OL	232MBO	Discrimination
29	4–4.3	4.7–5.0	6.4–6.8	232MBO/other
31	1.8–2.1	3.7–4.0	9.3–9.6	All
41	2.1–2.4	4.7–5.0	3.3–3.6	All
43	1.4–1.8	2.7–3.1	4.9–5.2	All
45	0.5–0.9	0.8–1.2	2.7–3.0	232MBO/other
57	0.5–0.9	8.8–9.1	7.4–7.7	All
69	≈0	2.4–2.7	2.0–2.4	331MBO/other
72	#	#	5.2–5.5	232MBO/other

#: Signal below the analytical detection limit.

m/z 31, m/z 41, m/z 43, m/z 57 and m/z 72. Results of break-up of the protonated alcohols as a function of the collision energy at a collision cell pressure of 1.5×10^{-4} hPa and experimental values of the appearance potentials are shown in Fig. 9 and Table 2, respectively. The last column of Table 2 shows the compounds, which can be distinguished by taking into account the estimated appearance potential of the fragment ions. One possibility to distinguish compounds could be to follow the ion at m/z 43 ion at two E_{CM} values, for example, at 2 eV (at which only ions at m/z 43 from 331MBO are observed) and at 4 eV (at which no ions at m/z 43 are observed for 232MBO).

4. Conclusion

A FA-TMS is a flexible tool to investigate isobaric and isomeric compounds in real-time. It has been shown that the protonated C_5 alcohol was only observed for 1P3OL, 232MBO and 331MBO, when using H_3O^+ reactant ions. H_3O^+ is the most widespread CI reactant ion, but produces essentially ions at m/z 69. The CID of this ion clearly showed that MBOs could be distinguished from pentenols by the calculation of ratios of ion signals at different m/z values (both fragments and parent). 331MBO was easily differentiated from the other methylbutenols and isoprene. Slight differences were observed between 232MBO and ISO and between (*Z*)2P1OL and the other two pentenols, but precision on ratios has to be improved to exploit these data. CID of ions at m/z 87 provided sufficiently different break-up patterns to discriminate 1P3OL, 232MBO and 331MBO. Even if the use of ions at m/z 87 suffers from a lack of sensitivity in the present instrumental configuration, the possible coupling of a drift tube instead of a flow tube to the TMS may overcome this problem.

However, even if different ways can be investigated to identify pure compounds, the study of mixtures remains difficult. Based on well-chosen ratios of ion signals at different m/z values, "binary mixture" curves can be obtained if these ion signals ratios are sufficiently different for the two compounds in the mixture. Tests were performed on the ratio $R_{29/41}$ from CID of the parent ion at m/z 69 of 1P3OL and 232MBO, with promising preliminary results. But the atmospheric interest stays limited since these two alcohols are rarely found together in air samples. The study of the parent ion at m/z 87 and its CID fragment ions should be of more interest for the analysis of these gases in mixtures.

Acknowledgements

The authors gratefully acknowledge the financial support of the Belgian Federal Science Policy (research project #MO/35/022). They also thank Dr. V. Riffault from Ecole des Mines de Douai (France) and the anonymous reviewers for their interesting comments.

References

[1] A. Guenther, C.N. Hewitt, D. Erickson, R. Fall, C. Geron, T. Graedel, P. Harley, L. Klinger, M. Lerdau, W.A. Mckay, T. Pierce, B. Scholes, R. Steinbrecher, R. Tallamraju, J. Taylor, P. Zimmerman, A global model of natural organic compound emissions, J. Geophys. Res. 100 (D5) (1995) 8873–8892.
[2] C. Granier, P. Artaxo, C.E. Reeves, Emissions of Atmospheric Trace Compounds, Kluwer Academic Publishers, The Netherlands, 2004.
[3] A.G. Carlton, C. Wiedinmyer, J.H. Kroll, A review of secondary organic aerosol (SOA) formation from isoprene, Atmos. Chem. Phys. Discuss. 9 (2009) 8261–8305.
[4] M. Kanakidou, J.H. Seinfeld, S.N. Pandis, I. Barnes, F.J. Dentener, M.C. Facchini, R. Van Dingenen, B. Ervens, A. Nenes, C.J. Nielsen, E. Swietlicki, J.P. Putaud, Y. Balkanski, S. Fuzzi, J. Horth, G.K. Moortgat, R. Winterhalter, C.E.L. Myhre, K. Tsigaridis, E. Vignati, E.G. Stephanou, J. Wilson, Organic aerosol and global climate modeling: a review, Atmos. Chem. Phys. 5 (2005) 1053–1123.
[5] T.M. Ruuskanen, H. Hakola, M.K. Kajos, H. Heelén, V. Tarvainen, J. Rinne, Volatile organic compound emissions from Siberian larch, Atmos. Env. 41 (2007) 5807–5812.
[6] G.W. Schade, A.H. Goldstein, Fluxes of oxygenated volatile organic compounds from a ponderosa pine plantation, J. Geophys. Res. 106 (D3) (2001) 3111–3123.
[7] G.W. Schade, A.H. Goldstein, D.W. Gray, M.T. Lerdau, Canopy and leaf level emissions of 2-methyl-3-buten-2-ol from a ponderosa pine plantation, Atmos. Env. 34 (2000) 3535–3544.
[8] P.D. Goldan, W.C. Kuster, F.C. Fehsenfeld, S.A. Montzka, The observation of a C_5 alcohol emission in a North American pine forest, Geophys. Res. Lett. 20 (1993) 1039–1042.
[9] M.C. Hansen, R.S. Defries, J.R.G. Townshend, R. Sohlberg, Global land cover classification at 1 km spatial resolution using a classification tree approach, Int. J. Remote Sens. 21 (2000) 1331–1364.
[10] A.L. Steiner, S. Tonse, R.C. Cohen, A.H. Goldstein, R.A. Harley, Biogenic 2-methyl-3-buten-2-ol increases regional ozone and HO_x sources, Geophys. Res. Lett. 34 (2007), doi:10.1029/2007GL030802.
[11] R. Atkinson, J. Arey, Gas-phase tropospheric chemistry of biogenic volatile organic compounds: a review, Atmos. Env. 37 (S2) (2003) 197–219.
[12] R. Atkinson, J. Arey, Atmospheric degradation of volatile organic compounds, Chem. Rev. 103 (2003) 4605–4638.
[13] A.W.H. Chan, M.M. Galloway, A.J. Kwan, P.S. Chhabra, F.N. Keutsch, P.O. Wennberg, R.C. Flagan, J.H. Seinfeld, Photooxidation of 2-methyl-3-buten-2-ol (MBO) as a potential source of secondary organic aerosol, Env. Sci. Technol. 43 (2009) 4647–4652.
[14] G. König, M. Brunda, H. Puxbaum, C.N. Hewitt, S.C. Duckham, J. Rudolph, Relative contribution of oxygenated hydrocarbons to the total biogenic VOC emissions of selected mid-European, agricultural and natural plant species, Atmos. Env. 29 (1995) 861–874.
[15] R. Fall, T. Karl, A. Jordan, W. Lindinger, Biogenic C_5 VOCs: release from leaves after freeze–thaw wounding and occurrence in air at a high mountain observatory, Atmos. Env. 35 (2001) 3905–3916.
[16] A.C. Heiden, K. Kobel, M. Komenda, R. Koppmann, M. Shao, J. Wildt, Toluene emissions from plants, Geophys. Res. Lett. 26 (1999) 1283–1286.
[17] M. Lerdau, M. Keller, Controls on isoprene emission from trees in a subtropical dry forest, Plant Cell Env. 20 (1997) 569–578.
[18] D.J. Barket Jr., J.M. Hurst, T.L. Couch, A. Colorado, P.B. Shepson, D.D. Riemer, A.J. Hills, E.C. Apel, R. Hafer, B.K. Lamb, H.H. Westberg, C.T. Farmer, E.R. Stabenau, R.G. Zika, Intercomparison of automated methodologies for determination of ambient isoprene during the PROPHET 1998 summer campaign, J. Geophys. Res. 106 (D20) (2001) 24301–24313.
[19] A. Guenther, A. Hills, Eddy covariance measurement of isoprene fluxes, J. Geophys. Res. 103 (1998) 13145–13152.
[20] H. Hakola, V. Tarvainen, J. Bäck, H. Ranta, B. Bonn, J. Rinne, M. Kulmala, Seasonal variation of mono- and sesquiterpene emission rates of Scots pine, Biogeosciences 3 (2006) 93–101.
[21] V. Tarvainen, H. Hakola, H. Hellén, J. Bäck, P. Hari, M. Kulmala, Temperature and light dependence of the VOC emissions of Scots pine, Atmos. Chem. Phys. 5 (2005) 989–998.
[22] P. Harley, V. Fridd-Stroud, J. Greenberg, A. Guenther, P. Vasconcellos, Emission of 2-methyl-3-buten-2-ol by pines: a potentially large natural source of reactive carbon to the atmosphere, J. Geophys. Res. 103 (D19) (1998) 25479–25486.
[23] A. Guenther, P. Zimmerman, L. Klinger, J. Greenberg, C. Ennis, K. Davis, W. Pollock, H. Westberg, G. Allwine, C. Geron, Estimates of regional natural volatile organic compound fluxes from enclosure and ambient measurements, J. Geophys. Res. 101 (D1) (1996) 1345–1359.
[24] R. Holzinger, A. Lee, K.T.U. Paw, A.H. Goldstein, Observations of oxidation products above a forest imply biogenic emissions of very reactive compounds, Atmos. Chem. Phys. 5 (2005) 67–75.
[25] T.G. Karl, C. Spirig, J. Rinne, C. Stroud, P. Prevost, J. Greenberg, R. Fall, A. Guenther, Virtual disjunct eddy covariance measurements of organic compound fluxes from a subalpine forest using proton transfer reaction mass spectrometry, Atmos. Chem. Phys. 2 (2002) 279–291.
[26] J. Williams, U. Pöschl, P.J. Crutzen, A. Hansel, R. Holzinger, C. Warneke, W. Lindinger, J. Lelieveld, An atmospheric chemistry interpretation of mass scans obtained from a proton transfer mass spectrometer flown over the tropical rainforest of Surinam, J. Atmos. Chem. 38 (2001) 133–166.
[27] C. Warneke, J.A. de Gouw, E.R. Love joy, P.C. Murphy, W.C. Kuster, R. Fall, Development of proton-transfer ion trap-mass spectrometry: on-line detection and identification of volatile organic compounds in air, J. Am. Soc. Mass Spectrom. 16 (2005) 1316–1324.
[28] K.P. Wyche, R.S. Blake, A.M. Ellis, P.S. Monks, T. Brauers, R. Koppmann, E.C. Apel, Technical note: performance of chemical ionization reaction time-of-flight mass spectrometry (CIR-TOF-MS) for the measurement of atmospherically significant oxygenated volatile organic compounds, Atmos. Chem. Phys. 7 (2007) 609–620.
[29] F. Dhooghe, C. Amelynck, J. Rimetz-Planchon, N. Schoon, F. Vanhaecke, Flowing afterglow selected ion flow tube (FA-SIFT) study of ion/molecule reactions in support of the detection of biogenic alcohols by medium-pressure chemical ionization mass spectrometry techniques, Int. J. Mass Spectrom. 285 (2009) 31–41.
[30] N. Schoon, C. Amelynck, E. Debie, P. Bultinck, E. Arijs, A selected ion flow tube study of the reactions of H_3O^+, NO^+ and $O_2^{\bullet+}$ with a series of C_5, C_6 and C_8 unsaturated biogenic alcohols, Int. J. Mass Spectrom. 263 (2007) 127–136.
[31] T.G. Custer, S. Kato, R. Fall, V.M. Bierbaum, Negative-ion, CIMS: analysis of volatile leaf wound compounds including HCN, Int. J. Mass Spectrom. 223–224 (2003) 427–446.

[32] T.G. Custer, S. Kato, R. Fall, V.M. Bierbaum, Negative ion mass spectrometry and the detection of carbonyls and HCN from clover, Geophys. Res. Lett. 27 (2000) 3849–3852.
[33] C. Warneke, J.A. de Gouw, W.C. Kuster, P.D. Goldan, R. Fall, Validation of atmospheric VOC measurements by proton-transfer-reaction mass spectrometry using a gas-chromatographic preseparation method, Env. Sci. Technol. 37 (2003) 2494–2501.
[34] K.R. Jennings, The changing impact of the collision-induced decomposition of ions on mass spectrometry, Int. J. Mass Spectrom. 200 (2000) 479–493.
[35] M.M.L. Steeghs, E. Crespo, F.J.M. Harren, Collision induced dissociation study of 10 monoterpenes for identification in trace gas measurements using the newly developed proton-transfer reaction ion trap mass spectrometer, Int. J. Mass Spectrom. 263 (2007) 204–212.
[36] T. Karl, F. Harren, C. Warneke, J. De Gouw, C. Grayless, R. Fall, Senescing grass crops as regional sources of reactive volatile organic compounds, J. Geophys. Res. 110 (2005), doi:10.1029/2005JD005777.
[37] C. Warneke, J.A. de Gouw, E.R. Lovejoy, P.C. Murphy, W.C. Kuster, R. Fall, Development of proton-transfer ion trap-mass spectrometry: on-line detection and identification of volatile organic compounds in air, J. Am. Soc. Mass Spectrom. 16 (2005) 1316–1324.
[38] P. Prazeller, P.T. Palmer, E. Boscaini, T. Jobson, M. Alexander, Proton transfer reaction ion trap mass spectrometer, Rapid Commun. Mass Spectrom. 17 (2003) 1593–1599.
[39] L.H. Mielke, D.E. Erickson, S.A. McLuckey, M. Müller, A. Wisthaler, A. Hansel, B. Shepson, Development of a proton-transfer reaction-linear ion trap mass spectrometer for quantitative determination of volatile organic compounds, Anal. Chem. 80 (2008) 8171–8177.
[40] A. Colorado, D.J. Barket Jr., J.M. Hurst, P.B. Shepson, A fast response method for determination of atmospheric isoprene using quadrupole ion trap mass spectrometry, Anal. Chem. 70 (1998) 5129–5135.
[41] T. Reiner, T.O. Möhler, F. Arnold, Improved atmospheric trace gas measurements with an aircraft-based tandem mass spectrometer: ion identification by mass-selected fragmentation studies, J. Geophys. Res. 103 (D23) (1998) 31309–31320.
[42] O. Möhler, Th. Reiner, F. Arnold, A novel aircraft-based tandem mass spectrometer for atmospheric ion and trace gas measurements, Rev. Sci. Instrum. 64 (1993) 1199–1207.
[43] J. Auld, D.R. Hastie, Tandem mass spectrometry and multiple reaction monitoring using an atmospheric pressure chemical ionization triple quadrupole mass spectrometer for product identification in atmospherically important reactions, Int. J. Mass Spectrom. 282 (2009) 91–98.
[44] F. Muntean, P.B. Armentrout, Guided ion beam study of collision-induced dissociation dynamics: integral and differential cross sections, J. Chem. Phys. 115 (2001) 1213–1228.
[45] P.J. Marinelli, J.A. Paulino, L.S. Sunderlin, P.G. Wenthold, J.C. Poutsma, R.R. Squires, A tandem selected ion flow tube—triple quadrupole instrument, Int. Mass Spectrom. Ion Proc. 130 (1994) 89–105.
[46] R.R. Squires, Advances in flowing afterglow and selected-ion flow tube techniques, Int. J. Mass Spectrom. Ion Proc. 118/119 (1992) 503–518.
[47] S.T. Graul, R.R. Squires, A flowing afterglow-triple quadrupole study of the mechanisms and intermediates in the gas-phase reactions of $CH_3OH_2^+$ with CH_3OH, J. Mass Spectrom. Ion Proc. 81 (1987) 183–202.
[48] D. Smith, N.G. Adams, An ion/ion afterglow plasma as a source of simple and clustered positive and negative ions, J. Phys. D: Appl. Phys. 13 (1980) 1267–1273.
[49] P.H. Dawson, The collision-induced dissociation of protonated water clusters studied using triple quadrupole, Int. J. Mass Spectrom. Ion Phys. 43 (1982) 195–209.
[50] P.H. Dawson, J.B. French, J.A. Buckley, D.J. Douglas, D. Simmons, The use of triple quadrupole for sequential mass spectrometry. 1. The instrument parameters, Org. Mass Spectrom. 17 (1982) 205–211.
[51] R.I. Martinez, S. Dheandhanoo, Instrument-independent CAD spectral databases: absolute cross-section measurements in QQQ instruments, J. Res. Nat. Bur. Stand. 92 (1987) 229–237.
[52] P.H. Dawson, J.B. French, J.A. Buckley, D.J. Douglas, D. Simmons, The use of triple quadrupole for sequential mass spectrometry. 2. A detailed case study, Org. Mass Spectrom. 17 (1982) 212–219.
[53] C. Amelynck, N. Schoon, T. Kuppens, P. Bultinck, E. Arijs, A selected ion flow tube study of the reactions of H_3O^+, NO^+ and O_2^+ with some oxygenated biogenic volatile organic compounds, Int. J. Mass Spectrom. 247 (2005) 1–9.
[54] D. Smith, A.M. Diskin, Y. Ji, P. Spanel, concurrent use of H_3O^+, NO^+ and O_2^+ precursor ions for the detection and quantification of diverse trace gases in the presence of air and breath by selected ion-flow tube mass spectrometry, Int. J. Mass Spectrom. 209 (2001) 81–97.
[55] P. Spanel, D. Smith, Selected ion flow tube-mass spectrometry: detection and real-time monitoring of flavours released by food products, Rapid Commun. Mass Spectrom. 13 (1999) 585–596.
[56] B. Munson, T.-M. Feng, H.D. Ward, R.K. Murray Jr., Isobutane chemical ionization mass spectra of unsaturated alcohols, Org. Mass Spectrom. 22 (1987) 606–609.
[57] P. Spanel, M. Pavlik, D. Smith, Reactions of H_3O^+ and OH^- ions with some organic molecules; applications to trace gas analysis in air, Int. J. Mass Spectrom. Ion Proc. 145 (1995) 177–186.
[58] P.B. Armentrout, K.M. Ervin, M.T. Rodgers, Statistical rate theory and kinetic energy-resolved ion chemistry: theory and applications, J. Phys. Chem. A 112 (2008) 10071–10085.
[59] S.D. Maleknia, T.L. Bell, M.A. Adams, PTR-MS analysis of reference and plant-emitted volatile organic compounds, Int. J. Mass Spectrom. 262 (2007) 203–210.
[60] M. Müller, L.H. Mielke, M. Breitenlechner, S.A. McLuckey, P.B. Shepson, A. Wisthaler, A. Hansel, MS/MS studies for the selective detection of isomeric biogenic VOCs using a Townsend Discharge Triple Quadrupole Tandem MS and a PTR-Linear Ion Trap MS, Atmos. Meas. Tech. Discuss. 2 (2009) 1837–1861.
[61] K. Buhr, S. van Ruth, C. Delahunty, Analysis of volatile flavour compounds by proton transfer reaction-mass spectrometry: fragmentation patterns and discrimination between isobaric and isomeric compounds, Int. J. Mass Spectrom. 221 (2002) 1–7.
[62] P.H. Dawson, A study of the collision-induced dissociation of $C_2H_5OH_2^+$ using various target gases, Int. J. Mass Spectrom. Ion Phys. 50 (1983) 287–297.